

Source mechanism of intermediate and deep earthquakes in southern Spain

E. Buorn, P. Coca, A. Udías & C. Lasá

Departamento de Geofísica, Universidad Complutense, Facultad Ciencias Fisicas, Madrid, Spain

Received 6 September 1996; accepted in revised form 30 June 1997

Key words: seismicity, source mechanism, intermediate and deep earthquakes, South Spain, subduction zone, delamination process

Abstract

Focal mechanisms of 10 intermediate-depth earthquakes ($30 < h < 150$ km) and one very deep ($h \cong 650$ km) which occurred in southern Spain and the Alboran Sea are studied in this paper. Distribution of epicenters with foci at intermediate depth shows a N–S alignment with a geometry parallel to the east of the Arc of Gibraltar. Focal mechanisms have been determined from first motion of P-wave and modeling wave forms of direct P arrivals. Most of the intermediate depth events present single source time functions with small time duration (smaller than 0.3 s) and only for the event of March 27, 1987 a complex source time function has been found. The very deep earthquake of March 8, 1990 has a complex focal mechanism with a long source time function (1.2 s) and two different fault-plane orientations. Scalar seismic moments and dimensions have been obtained from modeling and spectral analysis. The results are interpreted in terms of the seismotectonic framework of the region and suggest the existence of a vertical slab extending from 50 km to 150 km with strike N–S produced by a lithospheric delamination process. The existence of the very deep activity at 650 km of depth may be explained in terms of a block of lithospheric material that still cold and rigid, generates the very deep earthquakes.

Introduction

Seismic activity in southern Spain is associated with the plate boundary between Eurasia and Africa and is formed mostly by shallow earthquakes ($0 < h < 30$ km) with small to moderate magnitude ($M \leq 5$). However, earthquakes of intermediate ($30 < h < 150$ km) focal depth are also present in this area. Several authors have confirmed the existence of this intermediate depth seismicity that spreads out also through the Alboran Sea, Gulf of Cadiz and northern Morocco (Munuera, 1963; Hatzfeld, 1978; Hatzfeld and Frogneux, 1981; Grimison and Cheng, 1986; Buorn et al., 1988, 1991a; Seber et al., 1996). Also, sporadic very deep earthquakes ($h \cong 650$ km) occur in the region, in a small area, under south of Granada (Spain), with moderate to large magnitude ($5 < M < 7$) (Hodgson and Cock, 1956; Bonelli and Esteban Carrasco, 1957; Chung and Kanamori, 1976; Grimison and Cheng, 1986; Buorn et al., 1991b).

The occurrence of intermediate depth and very deep shocks in this area points to the existence of deep heterogeneities in the upper mantle and is a consequence of deep tectonics processes. Most papers dealing with the intermediate depth earthquakes of this region discuss only hypocentral data (Munuera, 1963; Hatzfeld, 1978; Seber et al., 1996) or a few fault plane solutions (Grimison and Cheng, 1986; Buorn et al., 1991a). Different tectonic models have been proposed for the origin of the deep seismic activity in this region such as deep fractures heterogeneities in the mantle, subduction process and continental lithospheric delamination (Hatzfeld and Frogneux, 1981; Grimison et al., 1986; Buorn et al., 1991; Seber et al., 1996). In this paper we present more accurate results from source mechanisms using wave form analysis for 10 intermediate depth and one very deep earthquake and their seismotectonic interpretation.

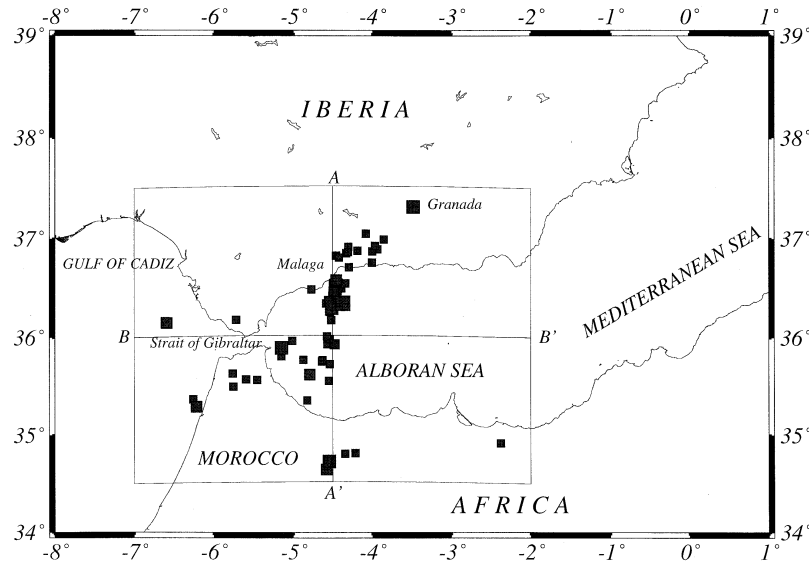


Figure 1. Distribution of epicenters with magnitude greater than 3.5, depth ($30 \text{ km} < h < 150 \text{ km}$) for the period 1975–1995 (I.G.N. Data File).

Distribution of intermediate depth foci

The distribution of epicenters with foci at intermediate depth ($30 \text{ km} < h < 150 \text{ km}$) for the period 1975–1995 and magnitudes greater than 3.5, in an area limited by longitudes 2° W and 7° W and latitudes 34° N and 37° N , is represented in Figure 1 (I.G.N. Data File). For this period due to the operation of upgraded seismological networks in Spain and Morocco, depth determination is thought to be more reliable. In this area no earthquakes with magnitude greater than 5.5, were recorded during this period. Epicenters are distributed in an approximately N–S alignment with a geometry parallel to the east of the Arc of Gibraltar, extending from the Málaga coast in South Spain, through the western part of the Alboran sea to the Morocco coast. Some epicenters are also located west of the Strait of Gibraltar, in the Gulf of Cádiz, but the most important concentration is to east of the Strait of Gibraltar.

A vertical cross-section (A–A') oriented in N–S direction, centered in 4.5° W and extended from 7° W to 2° W and another oriented in E–W direction (B–B'), centered in 36° N and with a width of 3° (from 34.5° N to 37.5° N) are shown in Figures 2a and 2b. The N–S cross-section shows that the maximum depth of foci is about 140 km, between 35.5° N and 36.5° N , which corresponds to Alboran sea between the Moroccan (35.5°) and Spanish coast (36.5°). This agrees with the results found by Seber et al. (1996). The E–

W cross-section shows the concentration of shocks at 4.5° W corresponding to a narrow zone striking with a N–S trend and with less than 100 km of width extending from 50 km to 150 km in depth. This important aspect of the geometry of the distribution of intermediate shocks is overlooked by Seber et al. (1996) who only show the N–S cross section which as shown in Figure 2a is not very illustrative. In their Figure 1, this N–S trend of the intermediate depth shocks is obscured by the plot of shallow shocks.

Focal mechanisms

Focal mechanisms of eleven earthquakes in the selected area of southern Spain and Alboran sea during the period 1986–1991, have been determined. Magnitudes are between 3.0 and 5.0 and depths between 58 and 100 km, only one event (March 8, 1990) have focus at very deep depth ($h=637 \text{ km}$) (Figure 3 and Table 1).

The distribution of the epicenters follows the general trend already mentioned for the intermediate depth events, in N–S direction, from Málaga coast to northern Morocco. Seven events are located in the Spanish coast and three in the Alboran sea. The very deep event (7) is located under Dúrcal, south of Granada (Spain).

Fault-plane solutions have been estimated from first motions of P-waves using the algorithm developed by Brüggen et al. (1980). Solutions obtained are shown

Table 1. Hypocentral data of earthquakes (I.G.N. Data File) used in this study. EH and EZ are given in km. N.st = number of stations.

No.	Date	Time (h:m:s)	Lat. (N)	Long. (W)	H (km)	RMS	EH	EZ	N.st.	MAG (IGN)
1	13-05-86	00:19:00.0	36° 36'	4° 29'	90	0.8	2	4	52	4.3
2	27-03-87	09:38:25.3	36° 47'	4° 06'	69	0.7	1	2	57	3.5
3	28-11-88	19:54:28.7	36° 18'	4° 34'	100	0.8	3	4	34	3.5
4	12-12-88	06:40:42.4	36° 17'	4° 34'	95	0.7	1	2	79	4.5
5	19-07-89	10:49:34.4	36° 38'	4° 26'	95	0.6	3	2	32	3.0
6	06-02-90	07:41:29.2	36° 34'	4° 31'	68	0.8	2	2	68	3.4
7	08-03-90	01:37:12.2	37° 00'	3° 60'	637	0.7	6	3	45	5.0
8	13-04-90	22:17:13.7	35° 36'	4° 49'	89	0.9	2	5	81	3.9
9	02-05-90	16:40:26.9	36° 32'	4° 31'	95	0.8	2	3	83	4.2
10	18-11-90	15:26:11.4	36° 25'	4° 35'	85	0.8	2	3	53	3.4
11	25-08-91	13:04:00.1	36° 49'	4° 29'	58	0.8	1	2	82	3.8

in Table 2, that includes values of estimations of standard deviations of T and P axes and fault planes orientation, obtained from the covariance matrix of the solution (see Brillinger et al. (1980) and Udías and Buforn (1988), for interpretation of these estimations). Data used correspond to digital and analogic stations at regional distances (between 30 km and 600 km) located in the Iberian Peninsula and the Maghreb. Most of the solutions are based on data from more than 10 stations and solutions of events 5, 8, 9, 10 and 30 from more than 20 stations. Solutions are well constrained with small standard deviations with exception for shocks 3, 5, 6 and 10 that have only 10 observations.

Modeling P-wave forms

The method of modeling P-wave forms to study the seismic source is very useful in order to obtain better estimates of fault-plane orientation and focal depth, and to determine source time functions (STF) and seismic moments. However, the application of this method to waves recorded at regional distances ($100 < \Delta < 600$ km) presents some difficulties. The most important is the correct separation of source from propagation path effects. For these distances waves travel mostly through the crust and it is necessary to know in detail its structure which is not always possible. For deep and intermediate depth earthquakes, however, the problem can be solved by the use of only direct P rays, since these rays at the distances used travel almost vertically through the crust and are not much affected by its structure. Direct waves are first arrivals when foci are at intermediate and very deep depth and stations are rela-

tively close. In our study the rays used have incidence angles in the stations less than 20° corresponding to rays near the vertical.

This consideration has been used to model P waveforms of intermediate and very deep earthquakes of Table 1. Event 1 (May 13, 1986) included in Table 1 have only solution from polarities, because only 2 stations are digital; however, its solution is included in Annex I. The method applied is a modification of the method developed by Deschamps et al. (1980) for teleseismic distances. In both methods modeling P-wave forms is performed by visual comparison between the synthetic and observed seismograms. As first step, fault-plane solutions obtained from polarities are used to generate synthetic seismograms, that are compared with observed records. By modification of fault-plane orientations, depths and source time functions it is possible to obtain synthetic seismograms that best agree with the observed data. In our study, P-wave forms are modeled using a crust with a linear gradient of velocity over a halfspace with a different gradient of velocity that represents the upper mantle (Buforn et al., 1988). Depths have been fixed using those obtained in hypocentral determinations and the independent parameters are strike, dip, slip of fault plane and source time function.

Records used are from the digital seismological stations of the Spanish National Seismic Network (Red Sísmica Nacional, RSN) of Instituto Geográfico Nacional, Madrid (IGN). At the studied period the RSN was formed by 28 stations with vertical short period Kinematics seismographs with a frequency of 1 Hz and damping of 0.7, telemetered to a central station in

Table 2. Focal mechanisms estimated from first motion of P wave and from modeling of P-wave forms. P and T axes are given by the trend (F) and plunge (Θ) measured from N. Planes by their strike (φ), dip (δ) and slip (λ). N is the number of data used and score (correct over total number of observations).

No.	Φ	Θ	φ	δ	λ
1	T: 202 ± 14 P: 321 ± 18 N: 27	62 ± 14 49 ± 16 Score: 0.89	A: 335 ± 3 B: 87 ± 69	36 ± 16 74 ± 9	-152 ± 10 -123 ± 14
2	T: 349 ± 1 P: 157 ± 1 N: 12	59 ± 1 30 ± 1 Score: 0.95	A: 230 ± 3 B: 72 ± 1	15 ± 1 76 ± 1	110 ± 3 85 ± 1
3	T: 178 ± 64 P: 8 ± 18 N: 10	43 ± 55 47 ± 87 Score: 1.00	A: 205 ± 140 B: 93 ± 2	5 ± 15 88 ± 68	-157 ± 131 -85 ± 156
4	T: 182 ± 6 P: 283 ± 8 N: 30	26 ± 15 21 ± 15 Score: 0.93	A: 324 ± 7 B: 232 ± 7	55 ± 17 87 ± 14	176 ± 17 34 ± 17
5	T: 202 ± 43 P: 29 ± 24 N: 7	56 ± 9 33 ± 19 Score: 1.00	A: 134 ± 76 B: 296 ± 44	12 ± 56 79 ± 62	29 ± 42 94 ± 245
6	T: 24 ± 60 P: 179 ± 121 N: 12	67 ± 51 21 ± 31 Score: 1.00	A: 255 ± 154 B: 97 ± 170	25 ± 20 67 ± 44	111 ± 118 81 ± 155
Modelling	T: 12 P: 185 N: 10	68 22	A: 270 B: 97	23 64	96 88
7a	T: 268 ± 15 P: 84 ± 58 N: 40	17 ± 7 73 ± 6 Score: 0.95	A: 0 ± 41 B: 177 ± 12	28 ± 7 62 ± 7	-88 ± 40 -91 ± 120
7b	T: 43 ± 14 P: 142 ± 13 N: 15	34 ± 9 14 ± 8 Score: 0.80	A: 188 ± 13 B: 89 ± 14	56 ± 11 77 ± 4	165 ± 6 35 ± 12
8	T: 111 ± 19 P: 203 ± 16 N: 36	56 ± 28 1 ± 19 Score: 0.89	A: 263 ± 17 B: 142 ± 25	53 ± 19 55 ± 24	135 ± 35 47 ± 29
9	T: 234 ± 26 P: 333 ± 12 N: 22	71 ± 13 3 ± 11 Score: 0.78	A: 45 ± 11 B: 260 ± 19	45 ± 10 51 ± 12	116 ± 19 114 ± 15
Modelling	T: 236 P: 329 N: 8	66 1	A: 36 B: 260	49 51	123 59
10	T: 46 ± 29 P: 146 ± 125 N: 9	10 ± 3 46 ± 34 Score: 1.00	A: 175 ± 144 B: 285 ± 145	51 ± 19 67 ± 38	-30 ± 6 -137 ± 107
11	T: 246 ± 19 P: 58 ± 17 N: 30	55 ± 13 129 ± 17 Score: 0.83	A: 276 ± 20 B: 8 ± 15	38 ± 20 8 ± 13	3 ± 21 128 ± 20
Modelling	T: 250 P: 134 N: 9	30 37	A: 286 B: 191	39 86	-173 -52

Madrid. The system uses an AD converter of 12 bits, sampling rate of 0.01 s. (Tejedor and García, 1993). In Table 2 the fault-plane orientations are shown. When the modeling has modified the orientation, the new

solution is shown in Table 1, but in general, the differences are only of a few degrees. The method have certain ambiguities; for example, the width of the pulse is controlled by both the source time function and the

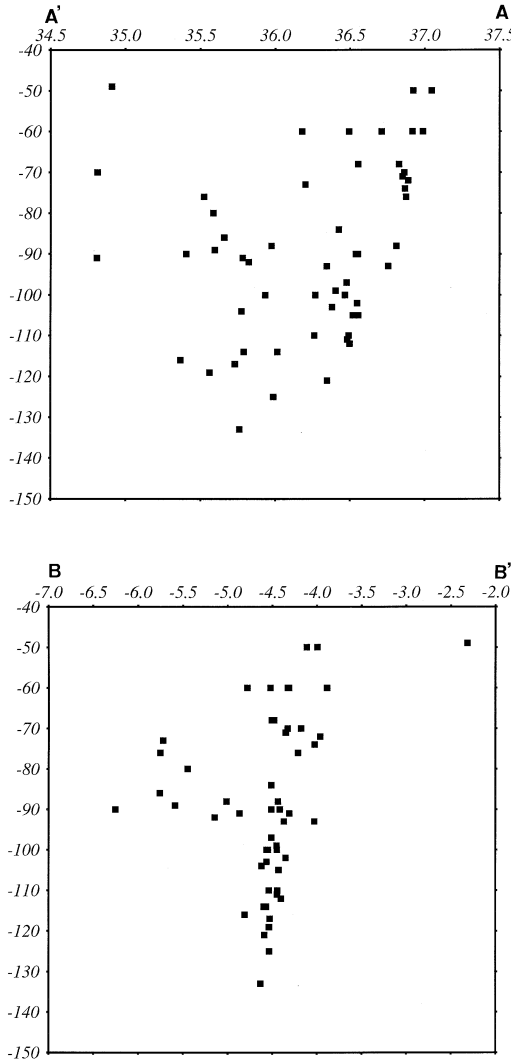


Figure 2. Vertical cross section from 40 km to 150 km corresponding to (a) profile AA' and (b) profile BB' in Figure 1 (I.G.N. Data File).

assumed Q values. At teleseismic distances and for shallow events usually the value along the path $T/Q \cong 1$ is assumed for attenuation effects (Carpenter, 1967). This is not possible at regional distances and Q values typical for the studied region must be used which in our case are not well known. For this reason we start the modeling using Q values obtained in other studies for southern Spain (Morales et al., 1991) and we modify these values to obtain, with the same source time function in all stations, synthetic wave forms that agree with the observed in each case. The Q values obtained in our study are between 50 and 600 for a range of depths between 60 and 600 km. This procedure is nec-

essary because it has been observed that the frequency content varies considerably for the same event from station to station pointing to different Q values for different paths. In any case, it is always possible to obtain the same synthetic seismograms using a short STF and lower Q values or a longer STF and higher Q values. In Figure 4 one example of this ambiguity is shown. Same synthetic records have been obtained for event 11 using a STF of 0.12 s duration and Q values of 85 at AFC and 120 at EJIF or a STF of 0.20 s and Q values of 200 in AFC and 400 in EJIF.

Deep earthquake ($h=637$ km)

Modeling of the earthquake of March 8, 1990 with focal depth of 637 km (event 7) is a special case. The shock was recorded at regional distances by 34 stations with clear P waves and very good azimuthal coverage. For our modeling study records from 16 digital stations were selected with clear P waves impulses. Records for three stations at epicentral distances of 175 km (EJIF), 412 km (GUD) and 647 km (ESEL) are shown in Figure 5. In all three records we can observe a first main pulse followed by three smaller ones (numbered as 1, 2, 3 and 4 in Figure 5). These three minor pulses are present in all stations and must be attributed to the source rather than to propagation effects. Since most stations are at distances less than the focal depth, rays travel almost vertically from the focus and there are no arrivals from reflexions at the crustal layers. The four arrivals may be interpreted as corresponding to a complex radiation source, formed by a main pulse followed by three smaller ones. Also it is possible, at most stations, to observe another 4 later arrivals (numbered as 1', 2', 3' and 4' in Figure 5) between 0.93 s and 2.7 s after the first group.

Fault plane solutions for main and second events are shown in Figure 6 and numerical values are listed in Table 2. The solution for the main event has a nearly vertical plane dipping 62° to the west and another nearly horizontal dipping 28° to the east both with strike N-S. Motion is purely dip-slip on both planes. The solution of the second event has a large component of strike-slip motion. One of the planes has strike N-S and dip to the west like the vertical plane of the first event. The second plane oriented in E-W direction is well constrained by a total of 15 observations.

Synthetic P-wave forms (Figure 6) have been obtained using a complex STF formed by 4 triangles with a total duration of 1.2 s. The orientation of fault planes for the main event have not changed from that

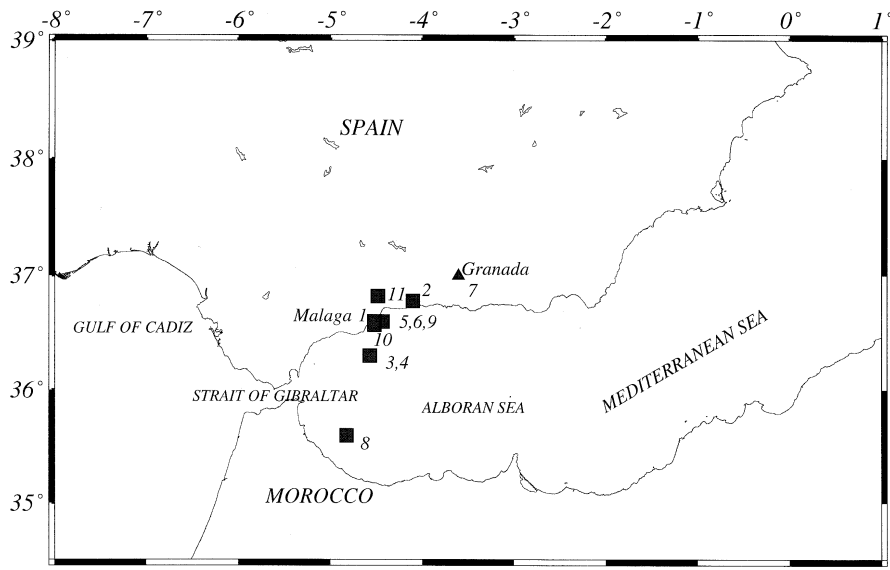


Figure 3. Distribution of epicenters of intermediate depth (squares) and deep depth (triangle) earthquakes for which the focal mechanism has been determined. Numbers correspond to Table 1.

Event 11 (25-08-91) $h=58$ km

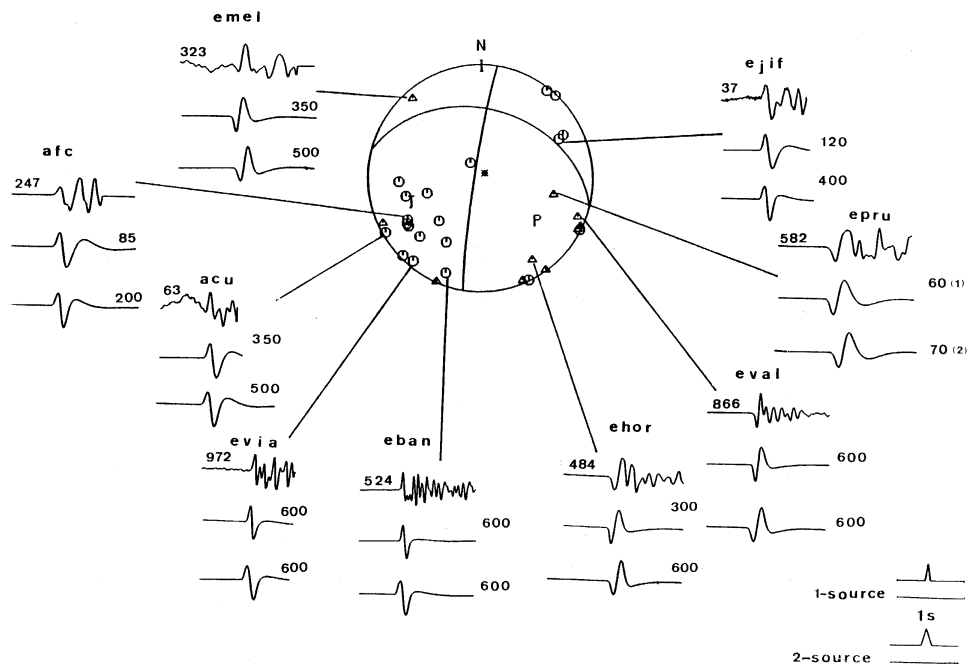


Figure 4. Fault-plane solution and modeling of P wave for shock 11 (August 25, 1991). Circles corresponds to compressions and triangles to dilatations. For each station the digital observed records of the direct P arrival are shown on top, middle and bottom traces correspond to synthetic records obtained with the two sources shown in the right corner. Right numbers correspond to Q values used in each station for the two sources. Horizontal scale (time) is shown in the source time function and is the same for all stations. Seismograms are normalized to maximum amplitude given in counts on each station (left numbers).

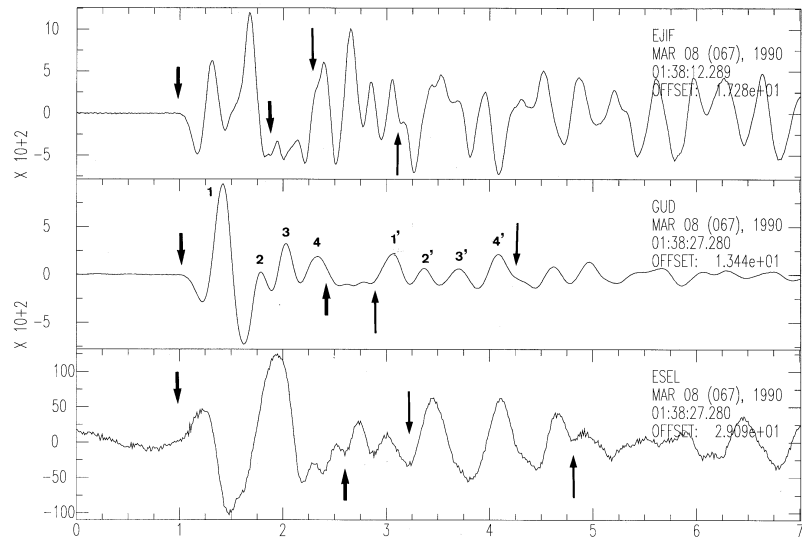


Figure 5. Records for the deep depth event of March 8, 1990. Arrows show the first and second group of arrivals numbered as 1, 2, 3 and 4 and 1', 2', 3' and 4'. Stations are at epicentral distance of 175 km, 412 km and 647 km respectively and azimuths of 71° , 173° and 241° .

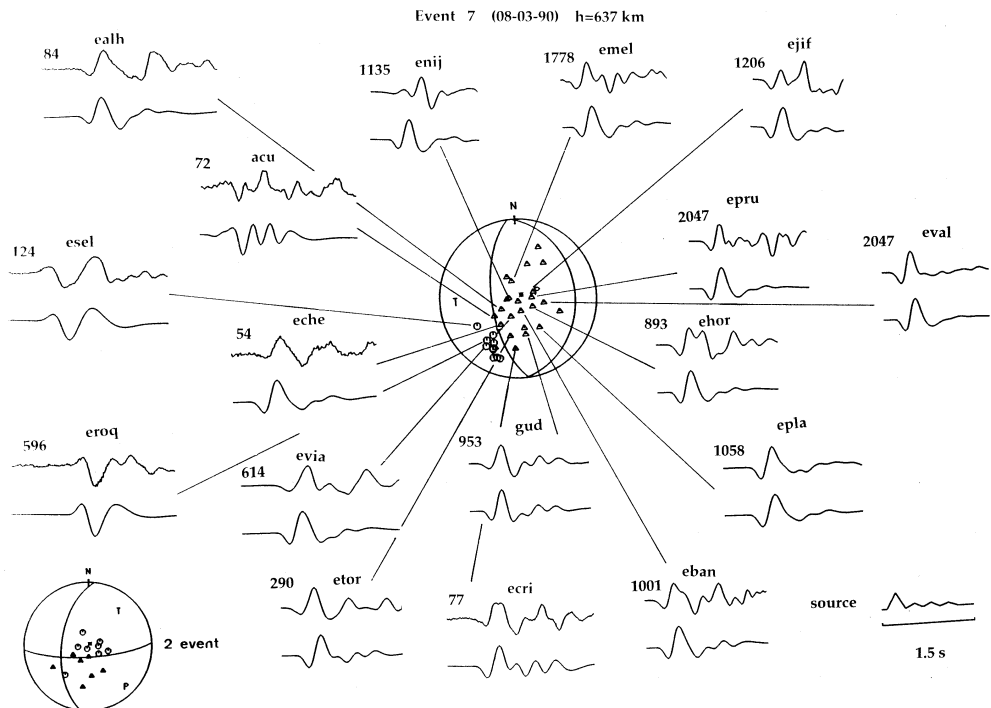


Figure 6. Fault-plane solution and P-wave modeling of event 7, March 8, 1990. Circles corresponds to compressions and triangles to dilatations. Top traces correspond to observed records and bottom traces to synthetic. Source time function is shown at bottom right corner. On the bottom left corner the fault-plane for second event is shown.

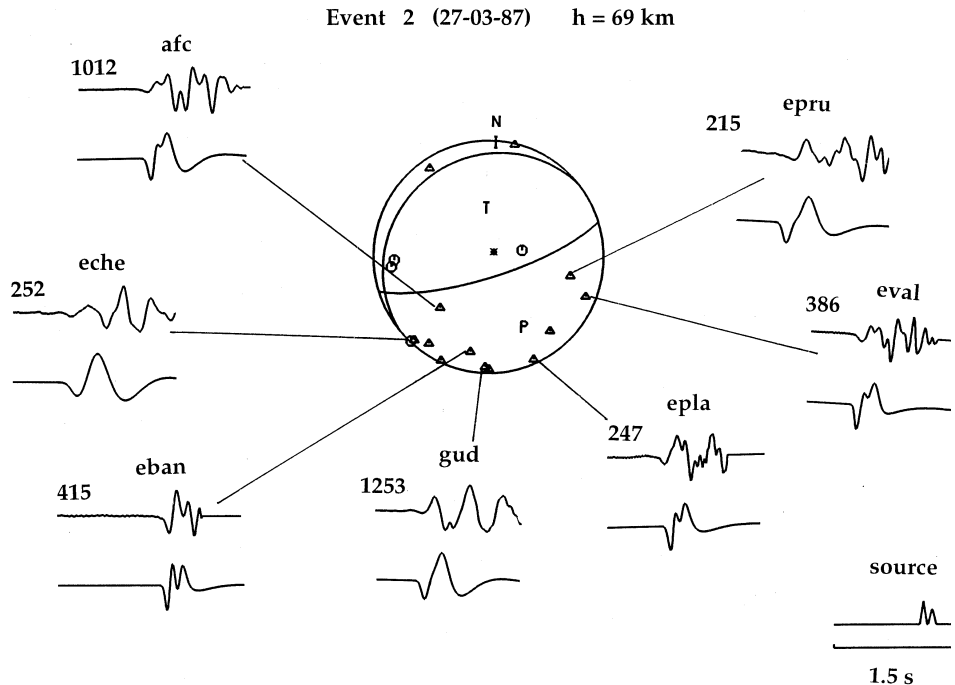


Figure 7. Fault-plane and P-wave modeling of event 2, March 27, 1987. Symbols are the same as those in Figure 6.

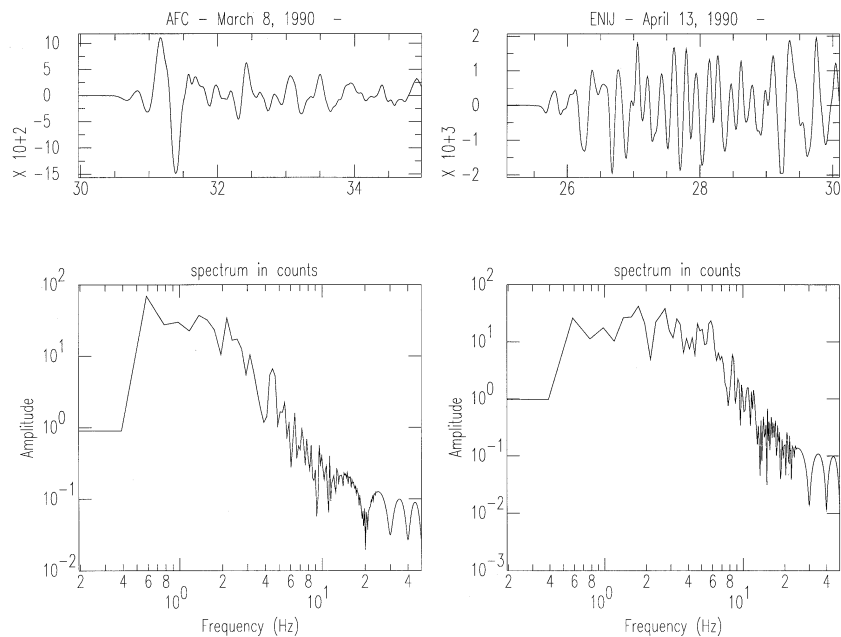


Figure 8. Examples of amplitude spectra. On top original records for very deep event 7 (March 8, 1990) and intermediate depth event 8 (April 13, 1990). The horizontal scale must be multiply by 0.01 s. Vertical scales are in counts.

obtained from P-wave polarities. For the source of the other three events, the orientation obtained from the P-wave polarities for the second event has been used. The different fault plane orientation is necessary in order to model the P-wave forms. The main event has a larger moment that represents about 70% of total scalar seismic moment, but the time duration is the same for all four events 0.3 s. From the source time duration and using a velocity rupture between 2.7 and 3.0 km/s a radius of about 3 km has been estimated. The complex source time function obtained for this shock, inspite of the large difference in magnitude, shows a similarity with the source estimated by Chung and Kanamori (1976) for the earthquake of March 29, 1954 ($M=7$; $h=650$ km) located practically at same place. They observed two very clear arrivals corresponding to two events with similar focal mechanism and a third less clear event that may have a different focal mechanism. Complex sources for small earthquakes ($M < 5$) have been found by Mori and Frankel (1990) and Kikuchi and Ishida (1993). The secondary arrivals (1', 2', 3' and 4') present in all stations may be interpreted in terms of converted S waves near the focus , but it has not been possible to model them. One possible explanation is a S to P wave conversion in the border of the rigid block that generates earthquakes at this depth. With this assumption, the dimensions of this block can be estimated from the time delay between the first and second groups of arrivals (1 s to 2.7 s). Using P and S wave velocities at the focus of 10.5 km/s and 5.8 km/s, the result for the radius of the block is about 26 km. This value is of the same order as the dimensions (36 km) found by Chung and Kanamori (1976) for the larger earthquake of 1954. This may be considered the maximum dimension of the block that generates deep earthquakes in this region.

Intermediate depth earthquakes

The results from the P-wave modeling for the 10 intermediate depth earthquakes are shown in Annex 1 and Table 2. Synthetic seismograms have been determined using the method described previously. Several STF and different Q values distribution with depth have been used. Solutions selected correspond to Q values increasing with depth and longer duration of STF according with magnitude of events. The number of stations is between 7 and 14 and most events have at least two quadrants covered by observations. The P-wave modeling did not change most of the solutions obtained from polarities.

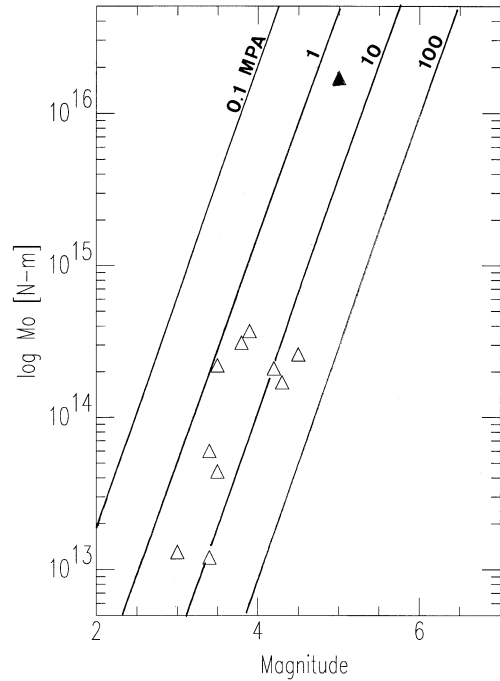


Figure 9. Plot of scalar seismic moment (M_0) versus magnitude of intermediate depth (white triangles) and very deep depth (black triangle) earthquakes.

Most STF correspond to a single impulse source, formed by a triangle with time duration between 0.06 s and 0.20 s (Annex 1). Synthetic forms agree well with observed P-wave forms. Event (2) (March 27, 1987) with magnitude 3.5, shows more complex P-wave forms with two arrivals present in all stations. The STF is formed by two triangles, the first larger but with small time duration than the second (Figure 7). This result shows that even small earthquakes may have complex wave radiation sources as has been shown by other authors as mentioned before.

Seismic moments and source dimensions were estimated from modeling and spectral analysis. In Figure 8, examples of typical spectra obtained for an event at intermediate depth (event 8) and the very deep (event 7) are shown. In Table 3 results from spectral analysis and modeling P-wave forms are compared. In most events scalar seismic moments obtained from spectral analysis and modeling P-wave forms are very similar. Both results only disagree for event 9, spectral analysis gives a value larger by a factor of 4 than from modeling. Values of seismic moments do not correspond exactly to those magnitudes given by the IGN for the earthquakes. The reason may be in the method used by the

Table 3. Scalar seismic moment (M_o) and dimensions (r) obtained from spectral analysis and from modeling method. Two values for radius in modelization corresponds to the two values of rupture velocity used (2.7–3.0 km/s.), $f(t)$ is duration in seconds of source time function.

No.	H (km)	M	$M_o * 10^{15}$ Nm	r (km)	$M_o * 10^{15}$ Nm	r (km)	$f(t)$ (s)
1	90	4.3	0.17 ± 0.03	0.53 ± 0.03			
2	65	3.5	0.22 ± 0.11	0.58 ± 0.10	0.28 ± 0.04	0.46–0.51	0.17
3	100	3.5	0.044 ± 0.008	0.62 ± 0.07	0.07 ± 0.01	0.49–0.54	0.18
4	95	4.5	0.26 ± 0.05	0.62 ± 0.04	0.13 ± 0.02	0.43–0.48	0.16
5	95	3.0	0.013 ± 0.003	0.51 ± 0.07	0.15 ± 0.05	0.43–0.48	0.16
6	68	3.4	0.06 ± 0.01	0.60 ± 0.07	0.07 ± 0.02	0.27–0.30	0.10
7	637	5.0	17.0 ± 1.0	1.98 ± 0.02	14.6 ± 3.4	3.24–3.60	1.20
8	89	3.9	0.37 ± 0.06	0.90 ± 0.05	1.60 ± 0.10	0.54–0.60	0.20
9	95	4.2	0.21 ± 0.03	0.74 ± 0.03	0.96 ± 0.03	0.54–0.60	0.20
10	85	3.4	0.012 ± 0.004	0.50 ± 0.02	0.010 ± 0.001	0.16–0.18	0.06
11	58	3.8	0.31 ± 0.05	0.51 ± 0.04	0.19 ± 0.02	0.22–0.24	0.08

IGN to estimate the magnitudes for local events, that is based in the amplitudes of L_g waves (Mézcua and Martínez Solares, 1983). L_g waves are not efficiently generated by intermediate depth earthquakes.

Scalar seismic moments (M_o) versus magnitudes are represented in Figure 9. It is possible to observe the problem in the magnitude estimation, several earthquakes have similar M_o , but magnitudes which range between 3 and 4. Most events have apparent stresses between 1 and 10 MPa (10 and 100 bars), values that agree with the results of Kanamori and Anderson (1975). The deep earthquake (black triangle) has also a similar value of apparent stress.

Corner frequencies were estimated by direct measurements of the spectra. Dimensions obtained from corner frequencies are very similar for all events, between 0.50 and 0.90 km, with the exception of the very deep depth earthquake (event 7) that has a radius of 2 km. These values are affected by the attenuation, which is very high and variable from place to place in the Betics region. For this reason, values obtained for dimensions are not very reliable.

Distribution of mechanisms

The focal mechanisms of the intermediate depth shocks determined from P wave modeling are represented in Figure 10a at their epicentral locations and in Figure 10b projected on a N–S vertical plane, the same as in Figure 2a. There are three groups of focal mechanisms. The first group is formed by shocks 1, 2, 3, 5 and 6; their solutions have one plane corresponding

to a vertical fault with strike in E–W direction and the other nearly horizontal with the same strike except for event 1 where the second plane dips 36° to the NNW. However, some of these mechanisms are not very well constrained, as we can see from Table 2, with large standard deviations (events 3, 5, 6). A second group is formed by shocks 8 and 9, both with mechanisms of reverse faulting with planes striking NE and NW respectively. In both cases one of the planes is nearly E–W. Shock 8 is located near the coast of Morocco south of the others shocks. The third group is formed by shocks 4, 10 and 11 and have different mechanisms. Shock 4 is the only one with large component of strike slip motion. Shock 10 has the only solution corresponding to normal faulting. Shock 11 has one vertical plane, but oriented N–S. The most common occurrence in all solutions, with the exception of shock 11, is the presence of a nearly vertical plane with strike in a general E–W direction and dip slip motion. Alternatively, for shocks 1, 2, 3, 5 and 6 motion could take place along nearly horizontal planes. Distribution with depth does not show any regularity (Figure 10b).

The orientation of the pressure (P) and tension (T) axes of the solutions are shown in Figure 11. In the horizontal projection only axes with plunge of P and T axes less than 45° are shown. In the vertical projection only axes with an angle less than 45° of the strike for the cross section plane are shown. The horizontal projections of P axes are rather scattered, some present a trend nearly perpendicular to the arc of Gibraltar (Figure 11a). Projected on a SE–NW vertical plane, most axes are nearly horizontal (Figure 11b). The horizontal projection of T axes have a very consistent trend

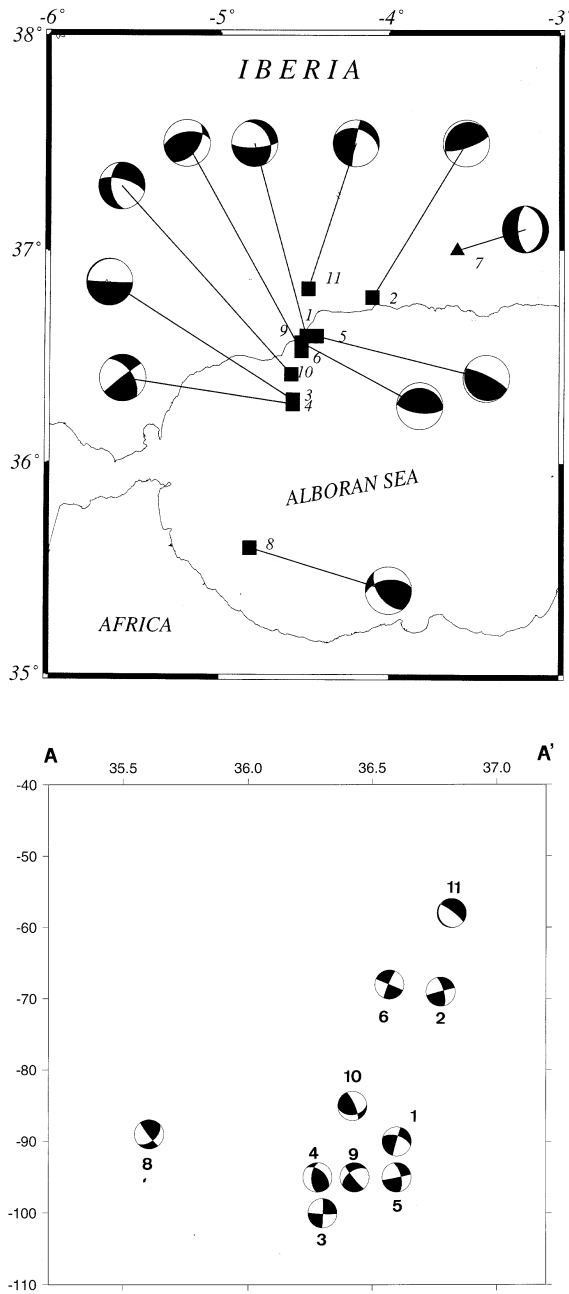


Figure 10. Horizontal and vertical projection of focal mechanisms. Plotted: (a) on a map of the region (10a) and (b) on a vertical N–S cross section (AA' of Figure 1).

on NNE direction (Figure 11c). Projected on a N–S vertical plane the T axes show a predominant nearly vertical direction and plunge to the south (Figure 11d).

The mechanism solution for the deep earthquake (shock 7) has planes oriented approximately N–S and

the P axis dips 45° to the east (Figure 10a). This mechanism agrees with the solutions found for the two other deep shocks of 1954 and 1973 (Buorn et al., 1991a, b) and is rotated 90° with respect to the predominant solutions found for the intermediate depth shocks.

Seismotectonic interpretation

Results of the seismicity distribution and source mechanisms of intermediate depth and deep earthquakes obtained here allow to propose certain interpretations regarding the structure and tectonic processes in this region. In first place, the solution for the deep earthquake (event 7) agrees with the idea, already proposed by several authors, that the origin of the deep seismic activity in this region is a detached block of lithospheric material sufficiently cold and rigid to generate earthquakes that has sunk to this depth (Udías and Lopez Arroyo, 1972; Udías et al., 1976; Chung and Kanamori, 1976; Grimison and Cheng, 1986; Buorn et al., 1991a). Recently Zeck (1996) has proposed from geological evidences for the origin of the slab, a N–S dipping subduction of Mesozoic Thethys lithosphere that broke off at about 24 My, connected with the eastward motion of Iberia/Europe relative to North America. However, this orientation of the subducted slab does not explain the consistent direction of the P axis found in the focal mechanisms solutions of the three deep earthquakes which dips to the east and not to the west or north–west. This orientation of the P axes does not have an easy explanation and it may not reflect the situation at the time of the subduction process. The difference in mechanism of the deep shocks with respect to the predominant mechanism of intermediate depth shocks and the absence of shocks between 150 and 600 km may show that, at present, there is no relation between the origin of deep shocks and those of intermediate depth.

The origin of intermediate depth earthquakes in this region has been explained in different ways. Some explanations postulate the existence of lithospheric material or heterogeneities in the upper mantle, deep fractures or some kind of subduction process (Hatzfeld and Frogneux, 1978; Grimison and Cheng, 1986; Buorn et al., 1988, 1991a). A discussion can be found in Buorn et al. (1995). Recently, Seber et al. (1996) have interpreted the structure responsible for the intermediate depth earthquakes in this region as produced by a process of delamination of continental lithosphere that had been previously engrossed. The delamination

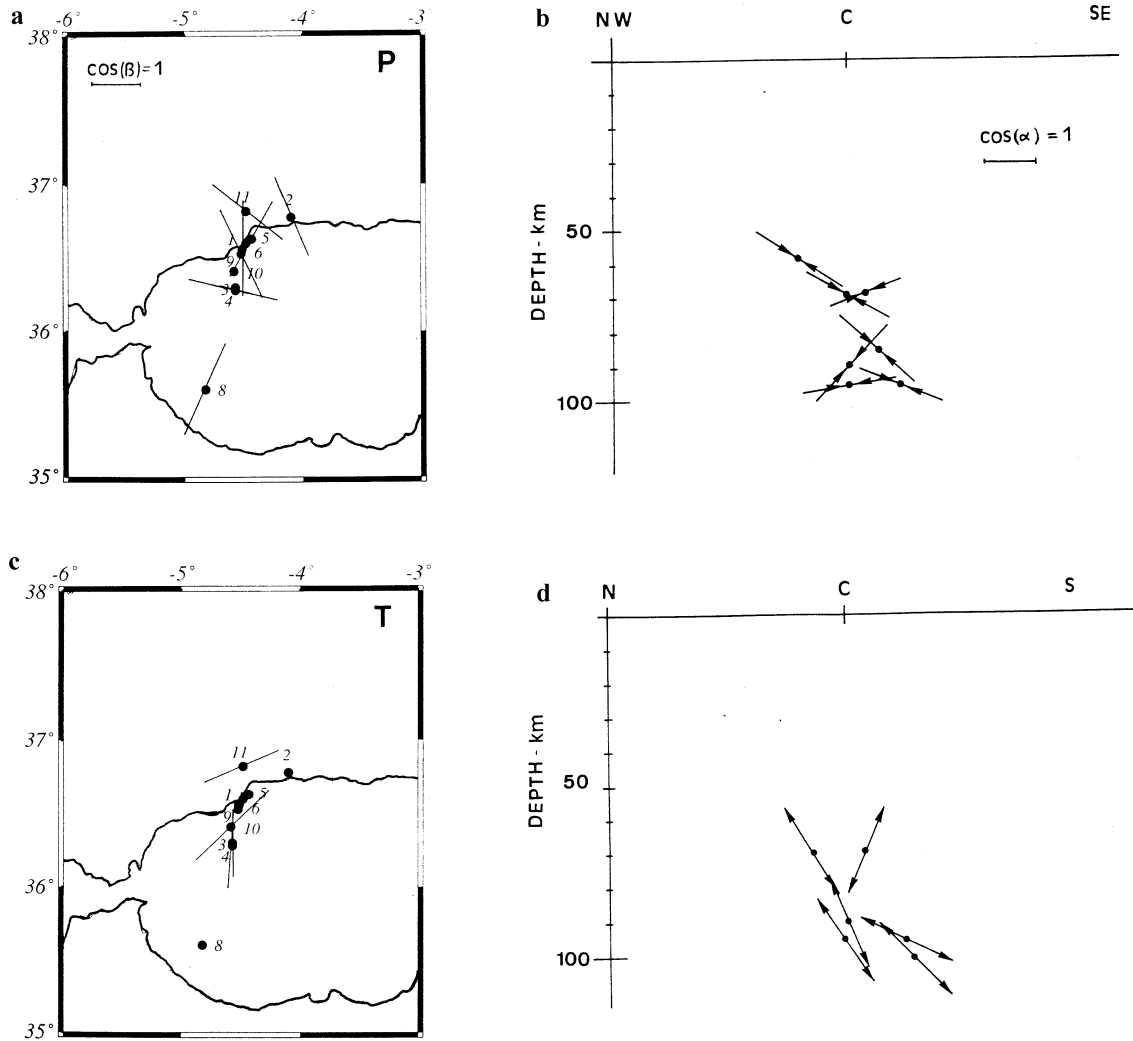


Figure 11. Plot of a horizontal projection of (a) P axes and (c) T axes. Projection on a vertical plane (b) of P axes on a plane of NW-SE trend and (d) of T axes on a plane with N-S trend. Length of lines is proportional to the cosine of plunge and cosine of the angle between the trend of the axes and the strike of the projection plane.

is a rather general term and in its strict sense (s.s.), it is used by these authors as a peeling off of the lithosphere and its sinking into the mantle with the peeling axis moving horizontally. The sunk lithosphere is replaced by upward motion of asthenospheric material. Houseman (1996) discusses two possible ways for removal of subcrustal lithosphere, namely, delamination (s.s.) and convecting thinning. In the latter the engrossed lithosphere sinks vertically into the mantle due to the gravitational instability created with respect to the lower density asthenosphere. Recognizing the complexity of the region under the Betics, Rif and Alboran basin,

Houseman considers that the situation is more easily explained in terms of a convecting thinning model.

Tomographic studies for this area show the existence of a high velocity region which extends from 50 km to 350 km overlaid by a low velocity region between 30 km and 50 km (Seber et al., 1996b). At higher depth, tomographic studies also show the well established existence of a large anomalous structure extending from 200 km to 700 km (Blanco and Spakman, 1993). This deep structure has higher velocities and encloses the location of the deep earthquakes. Blanco and Spakman (1993) also found a low velocity

region on top of the high velocity anomalous region at 200 km but their resolution may not be sufficient. There is, then, a disagreement between these two studies regarding the situation at the level from 150 km to 350 km. In both cases however, the resolution of these studies for this depth level may not be very good.

The distribution of hypocenters show in first place the existence of a clear N–S structure that extends in depth from 50 km to 150 km with a narrow width (less than 100 km) located at longitude 4.5° W (Figures 1, 2 and 3). All the intermediate shocks studied here fall on this structure. This particular structure is not easily explained by the general process of lithospheric delamination that may be present in the whole region.

The orientation of stress axes derived from the source mechanism of intermediate depth earthquakes show certain scattering that may be due to differences in local stress release. Inspite of the scatter tension axes show a predominant nearly vertical orientation (Figure 11c and 11d) while pressure axes are predominantly horizontal and with a greater scatter, some normal to the trend of the Gibraltar arc (Figure 11a and 11b). This orientation of the stress axes may indicate that the material at intermediate depth is under vertical tension probably due to its being stretched downward into the mantle and horizontal pressure. Since this is a relatively young process, it is reasonable that the material is at present subject to downward tensional stresses.

This situation would be more consistent with a model of convecting thinning with the lithospheric material sinking downward into the mantle than with a delamination (s.s.), where the lithosphere peels off at low angle. However, the area that has been studied is only a small part of the whole region which includes the Betics, Gulf of Cadiz, Alboran, Rif and Atlas where intermediate depth earthquakes also occur. It may happen that the delamination process has different characteristics from place to place inside the region. At this particular area, east of the straight of Gibraltar from south Spain to north Morocco, the material seems to sink almost vertically along a plane with N–S strike.

In conclusion, the observations of hypocentral distribution and source mechanism of earthquakes in the area, from south Spain to north Morocco, east of the Strait of Gibraltar suggest the existence of a vertical slab of lithospheric material extending from 50 km to 150 km with strike N–S which is being stretched downward. In a general context of lithospheric delamination in the wider region of South Spain, Alboran Sea and Morocco, these observations seem to be more

in agreement with a convecting thinning model at least for the particular area under study. At deeper depth ($h=650$ km) there exists a block of lithospheric material still cold and rigid that generates the very deep activity located in south Spain, probably sunk from a previous process of downward motion of lithosphere and included in a large anomalous body which extends from 200 km to 700 km in depth.

Acknowledgements

The authors wish to thank to Dr J. Mézcua, Instituto Geográfico Nacional, Madrid, for providing part of the data and J. M. Tejedor who provided the software necessary to read the Spanish digital stations records; Prof. R. Madariaga, from Institut de Physique du Globe, Paris and Prof. H. Kanamori, from California Institute of Technology, Pasadena, for their helpful comments. We also thanks an anonymous referee for his comments that helped in the final text. This work has been supported in part by the Dirección General de Investigación Científica y Tecnológica, project PB-92-0184, by the European Union, project EV-5V-CT94-0513 and by the Universidad Complutense, Madrid, project Becas Jaime del Amo. Publication 381, Department of Geophysics, Universidad Complutense de Madrid.

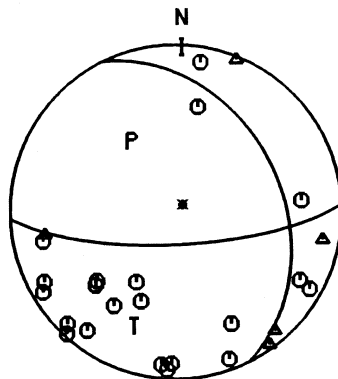
References

- Blanco, M. J. and Spakman, W., 1993, The P velocity structure of the mantle below the Iberian Peninsula: evidence for subducted lithosphere below south Spain, *Tectonophysics* **221**, 13–34.
- Bonelli, J. M. and Esteban Carrasco, L., 1957, *El sismo profundo de 29 de Marzo de 1954 en la falla de Motril*, Instituto Geográfico Nacional, Madrid, 28 pp.
- Brillinger, D. R., Udfás, A. and Bolt, B. A., 1980, A probability model for regional focal mechanism solution. *Bull. Seismol. Soc. Am.* **70**, 140–170.
- Buñorn, E., Udfás, A. and Mézcua, J., 1988, Seismicity and focal mechanisms in south Spain, *Bull. Seismol. Soc. Am.* **78**, 2008–2224.
- Buñorn, E., Udfás, A. and Madariaga, R., 1991, Intermediate and deep earthquakes in Spain, *Pageoph* **136**, 375–393.
- Buñorn, E., Udfás, A., Mézcua, J. and Madariaga, R., 1991, A deep earthquake under south Spain, 8 March 1990, *Bull. Seismol. Soc. Am.* **81**, 1403–1407.
- Buñorn, E., Sanz de Galdeano, C. and Udfás, A., 1995, Seismotectonics of the Ibero-Maghrebian region, *Tectonophysics* **248**, 247–261.
- Carpenter, E. W., 1967, Teleseismic signals calculated from underground, underwater and atmospheric explosions. *Geophysics* **32**, 17–32.

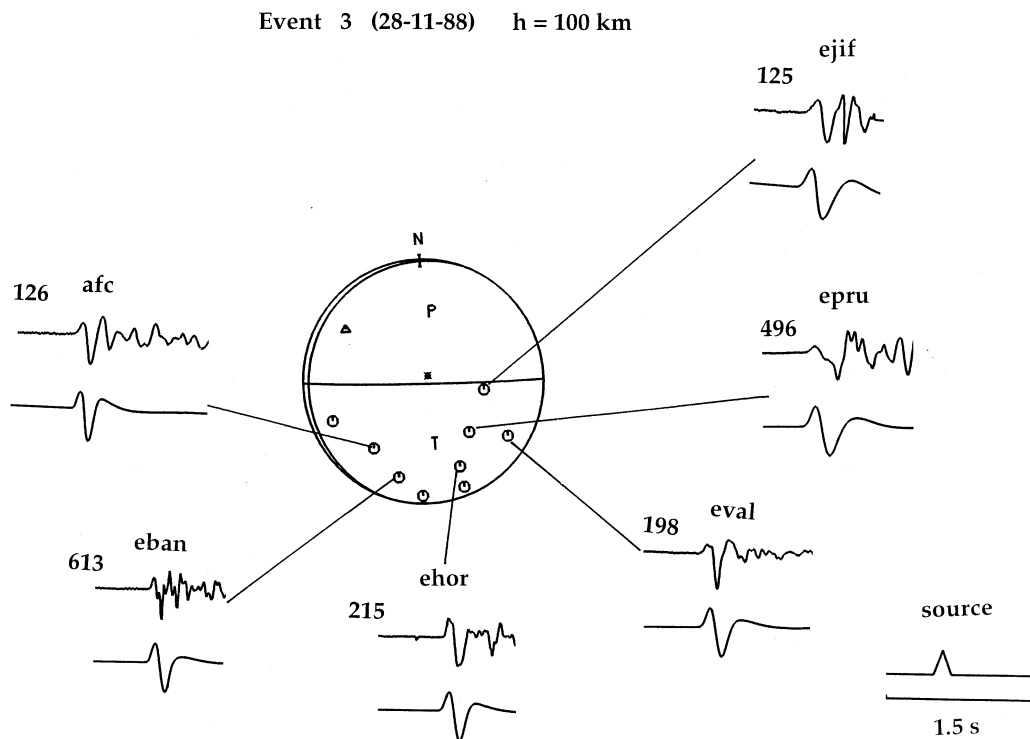
- Chung, W. and Kanamori, H., 1976, Source process and tectonic implications of the Spanish deep-focus earthquake of March 29, 1954, *Physics Earth and Plan. Int.* **13**, 85–96.
- Deschamps, A., Lyon-Caen, H. and Madariaga, R., 1980, Mise au point sur les méthodes de calcul de sismogrammes synthétiques de longue période, *Ann. Géophys.* **36**, 167–178.
- Grimison, N. and Cheng, W., 1986, The Azores-Gibraltar plate boundary: focal mechanisms, depths of earthquakes and the tectonic implications, *J. Geophys. Res.* **91**, 2029–2047.
- Hatzfeld, D., 1978, Etude sismotectonique de la zone de collision Ibero-Maghrébien. Doctoral Thesis, Université de Montpellier, 282 pp.
- Hatzfeld, D. and Frogneux, M., 1981, Intermediate deep seismicity in the western Mediterranean unrelated to subduction of oceanic lithosphere, *Nature* **292**, 443–445.
- Hodgson, J. H. and Cock, J. I., 1956, Direction of faulting in the deep focus Spanish earthquake of March 29, 1954, *Tellus* **8**, 321–328.
- Houseman, G., 1996, From mountains to basins. *Nature* **379**, 771–772.
- Kanamori, H. and Anderson, D. L., 1975, Theoretical basis of some empirical relations in seismology, *Bull. Seismol. Soc. Am.* **65**, 1073–1095.
- Kikuchi, M. and Ishida, M., 1993, Source retrieval for deep local earthquakes with broadband records, *Bull. Seism. Soc. Am.* **83**, 1855–1870.
- Mézcua, J. and Martínez Solares, J. M., 1983, Sismicidad del rea Ibero-Mogrebí. Instituto Geográfico Nacional, Madrid, 301 pp.
- Morales, J., Ibañez, J., Vidal, F., De Miguel, F., Alguacil, G. and Posadas, A., 1991, Q_c site dependence in the Granada Basin (Southern Spain), *Bull. Seism. Soc. Am.* **81**, 2486–2492.
- Mori, J. and Frankel, A., 1990, Source parameters for small events associated with the 1986 North Palm Springs, California, earthquake determined using empirical Green functions, *Bull. Seism. Soc. Am.* **80**, 278–285.
- Munuera, J. M., 1963, Datos básicos para un estudio de sismicidad en la región de la Península Ibérica, *Mem. Inst. Geog. Cat.*, Madrid **32**, 93 pp.
- Seber, D., Barazangi, M., Ibenbrahim, A. and Demnati, A., 1996, Geophysical evidence for lithospheric delamination beneath the Alboran Sea and Rift-Betic mountains, *Nature* **379**, 785–790.
- Tejedor, M. and García, O., 1993, *Funciones de transferencia de las estaciones de la Red Sísmica Nacional*. Instituto Geográfico Nacional, Madrid, 82 pp.
- Udías, A. and López Arroyo, A., 1972, Plate tectonics and the Azores-Gibraltar region, *Nature* **237**, 67–69.
- Udías, A. and Buforn, E., 1988, Single and joint fault-plane solutions from first motion data. In D. Doornbos (ed.), *Seismological Algorithms*, Academic Press, London, pp 443–453.
- Udías, A., López Arroyo, A. and Mézcua, J., 1976, Seismotectonics of the Azores-Alboran region, *Tectonophysics* **31**, 259–289.
- Zeck, H. P., 1996, Betic-Rif orogeny: subduction of Mesozoic Thethys lithosphere under eastward drifting Iberia, slab detachment shortly before 22 Ma, and subsequent uplift and extensional tectonics, *Tectonophysics* **254**, 1–16.

Annex

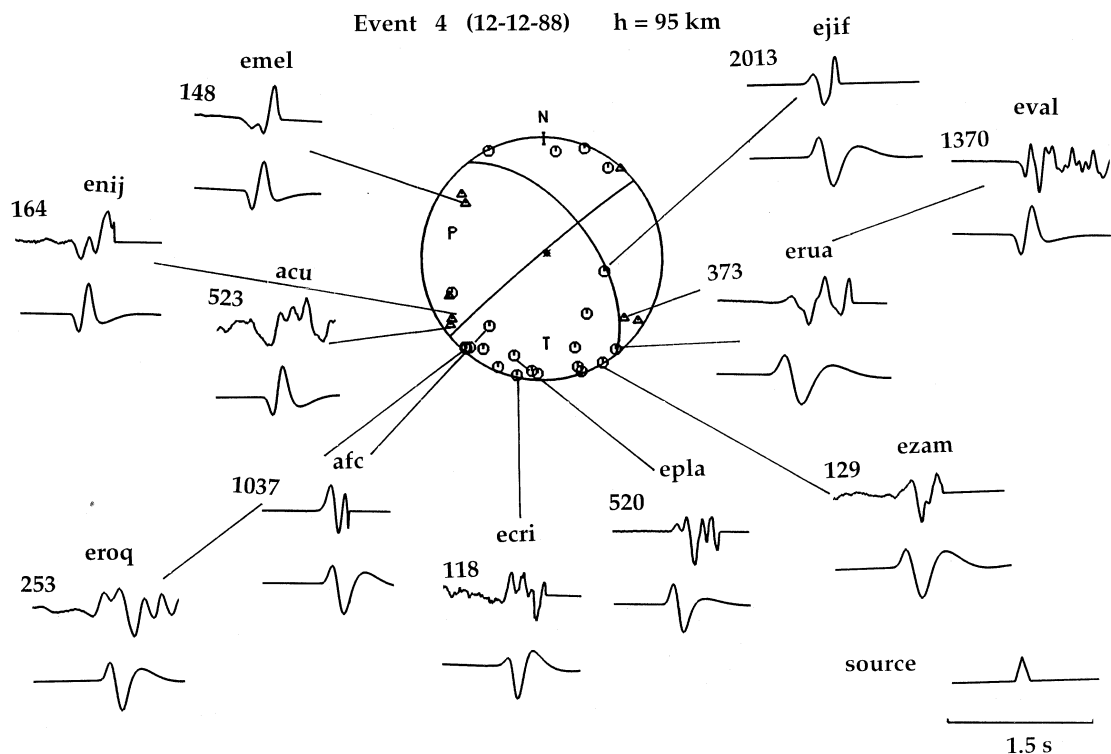
Event 1 (13-05-86) h=90 km



Annex 1. Fault-plane solutions and P-wave modeling of events studied in this paper. Circles corresponds to compressions and triangles to dilatations. Top traces correspond to observed records and bottom traces to synthetic. Source time function is shown at bottom right corner. Horizontal and vertical scales are the same that in Figure 4.

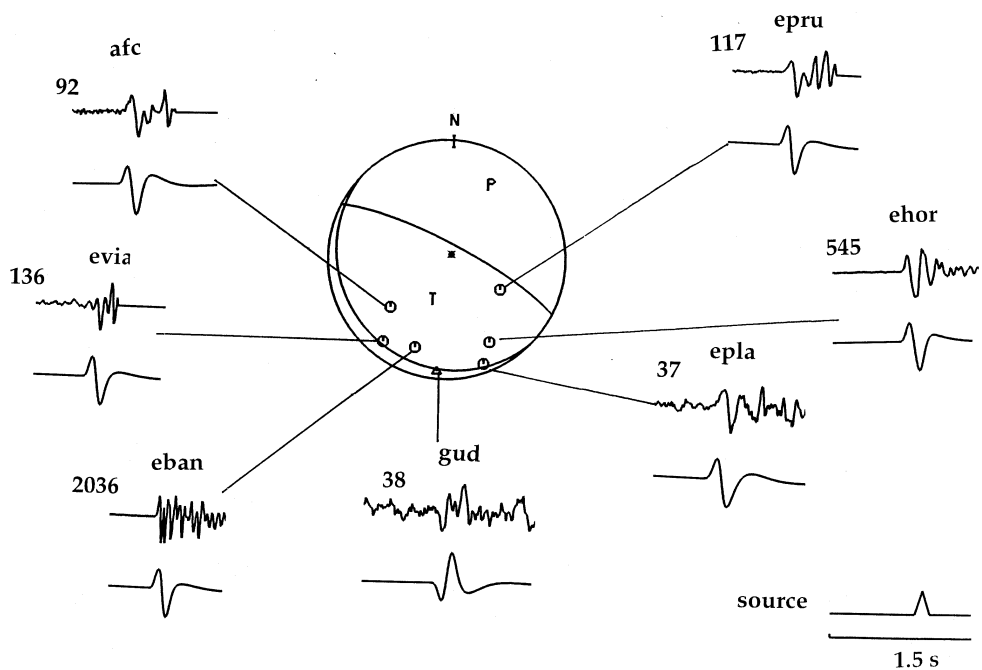


Annex 2.



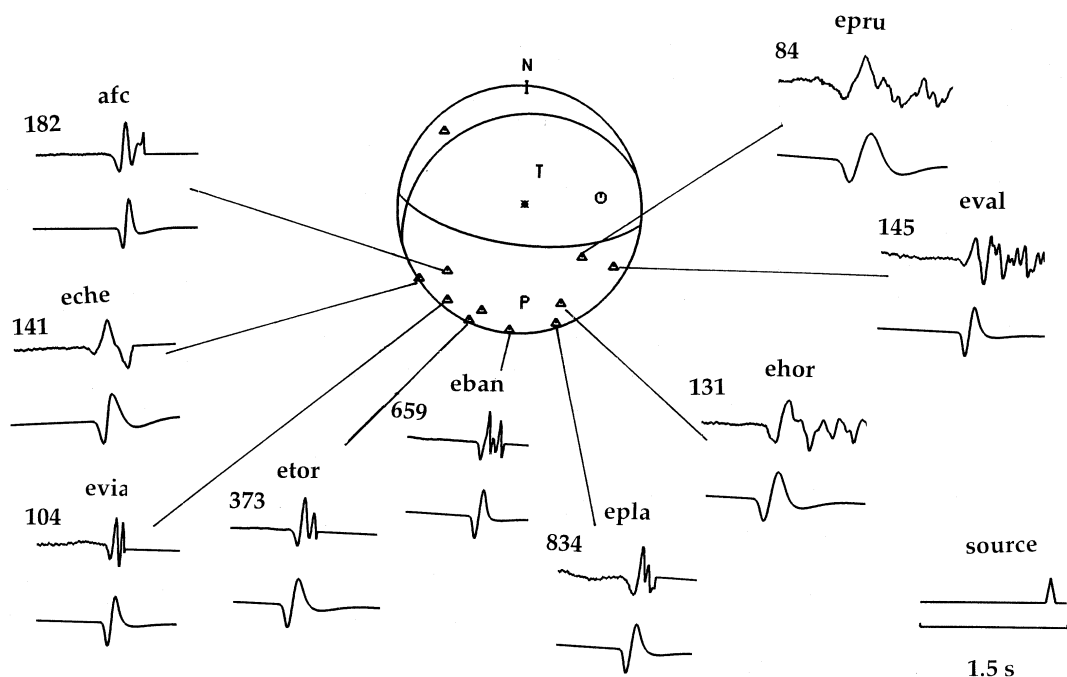
Annex 3.

Event 5 (19-07-89) h = 95 km

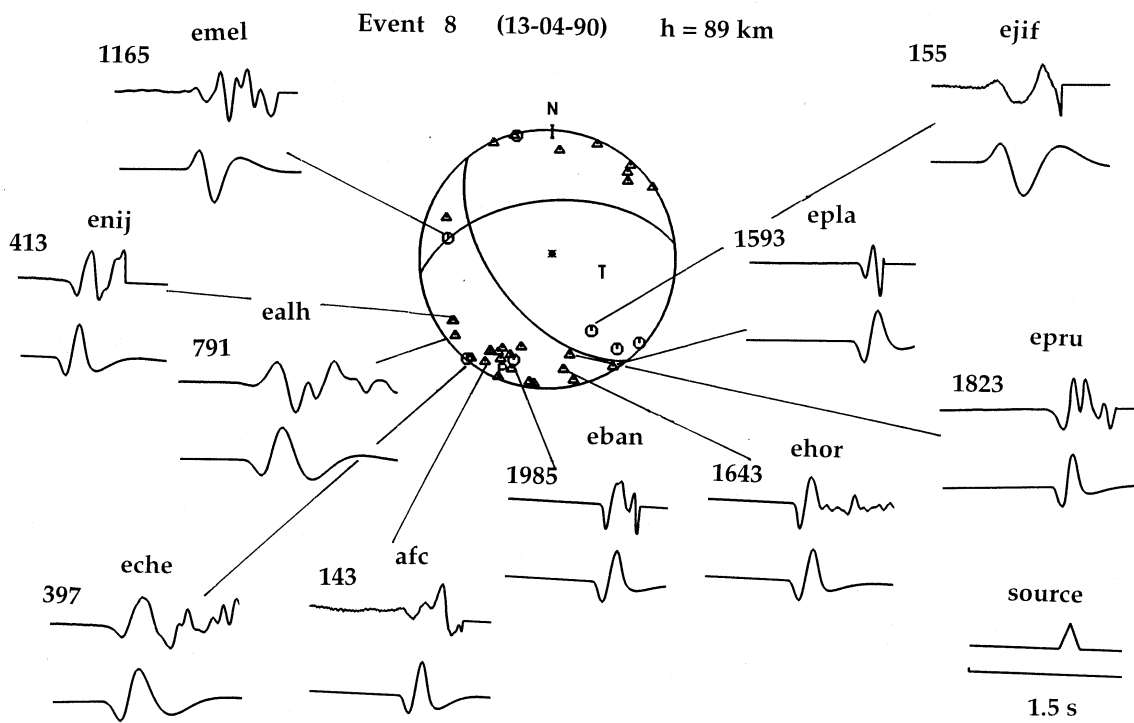


Annex 4.

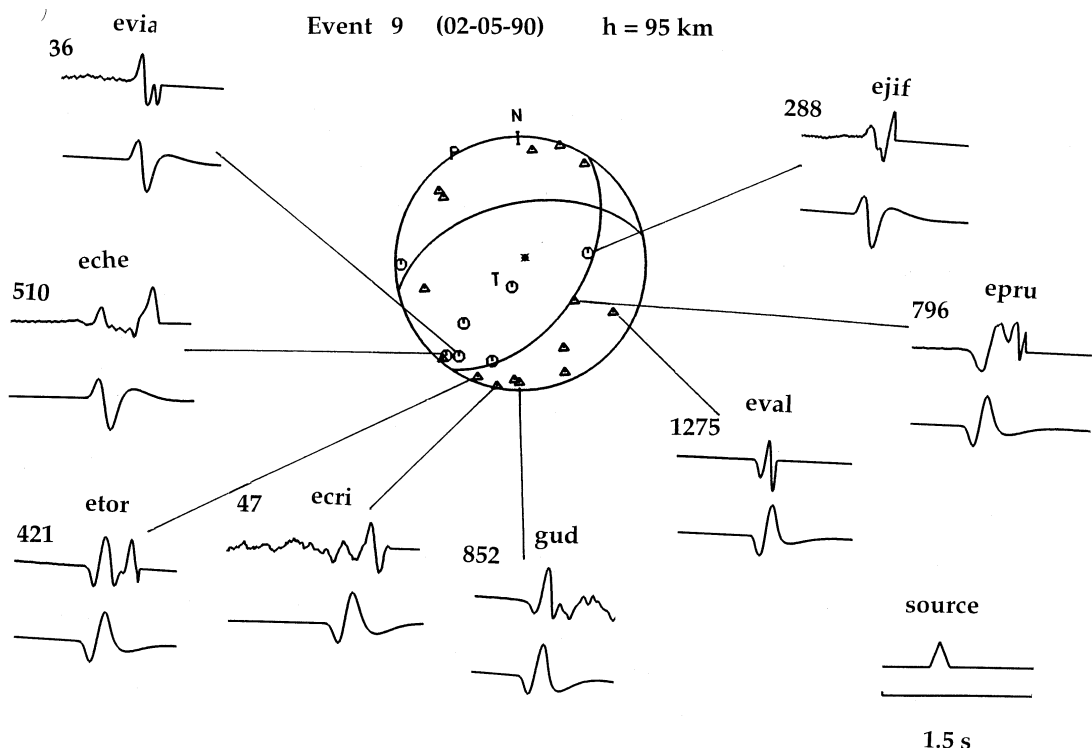
Event 6 (06-02-90) h = 68 km



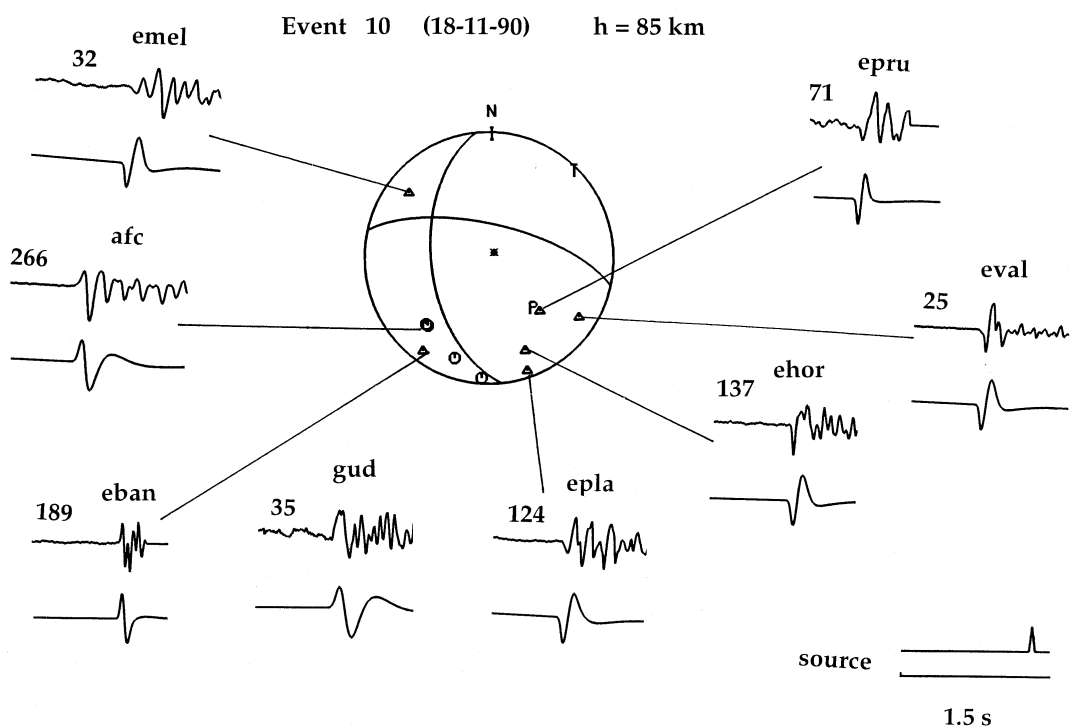
Annex 5.



Annex 6.



Annex 7.



Annex 8.